Electronic Supplementary Information

N-doped Graphitic Self-Encapsulation for High Performance Silicon Anodes in Lithium-Ion Batteries

Won Jun Lee,[ab] Tae Hoon Hwang,[c] Jin Ok Hwang,[ab] Hyun Wook Kim,[d] Joonwon Lim,[ab] Hu Young Jeong,[e] Jong Won Shim,[ab] Tae Hee Han,[f] Je Young Kim,[d] Jang Wook Choi, [*c] and Sang Ouk Kim[*ab]

[a]Center for Nanomaterials and Chemical Reactions, Institute for Basic Science (IBS), Daejeon 305-701 (Korea)

[b]Materials Science & Engineering, KAIST, Daejeon 305-701(Korea)

[c]Graduate School of EEWS (WCU), KAIST Institute NanoCentury, KAIST, Daejeon 305-701 (Korea)

[d]Battery R&D, LG Chem, Ltd. 104-1 Moonji-dong, Yuseong-gu, Daejeon 305-380 (Korea)

[e]UNIST Central Research Facility and School of Mechanical and Advanced Materials Engineering, UNIST, Ulsan 689-798 (Korea)

[f]Department of Organic and Nano Engineering, Hanyang University, Seoul 133-791 (Korea)

Thermogravimetric Analysis

Thermogravimetric analysis (TGA) was performed to check how much carbon encapsulant could be attached on the surface of Si particles. (see Figure S3†). N-CNT and N- graphene were before tested. N-CNT is thermally stable up to a temperature of 450°C (15.7 wt% weight loss at 600°C). In comparison to N-CNT, N-graphene starts to decompose at lower temperature ~350°C (23.4 wt% weight loss at 600°C) due to oxidation groups. For the graphitic carbon encapsulated Si samples, at 600°C, 0.73 wt%, 3.13 wt%, and 3.84 wt% for Si, Si@N-CNT, and Si@N-graphene are observed. From the weight loss amount, we could confirm amount of carbon attached to Si particles (15.3 wt% CNT for Si@N-CNT and 13.3 wt% for Si@N-graphene). These values are higher than we expected (9 wt% graphitic carbon encapsulants use for each material). The reason for Si loss might be the repeated filtering and washing process as described in experimental section. It is good evidence for stable adhesion of our encapsulation method and complete exhaustion of encapsulants.

Electrochemical Performance of Si@N-graphene

The electrochemical performances of the three electrodes were characterized in coin-type half-cells.). Galvanostatic mode was employed in the potential range of 0.01~1.2 V (versus Li^+/Li). Lithium foil was used for reference and counter electrodes simultaneously. The working electrode consists of 70 wt% of active material including carbon encapsulants, 15 wt% of super P, and 15 wt% of poly (acrylic acid) (PAA) binder. The active material loading densities for all of the three cases were ~0.8 mg/cm^2. Fig. S5a shows potential profiles during the first cycles measured at a current density of 100 mA/g. We note that if not indicated all the C-rates addressed in this work correspond to 1C values (2582 mA/g for Si@N-graphene, 2647 mA/g for Si only), which are different from practical charge/discharge durations. All

samples show the characteristic charge and discharge plateaus of Si at 0.1 and 0.4 V versus Li/Li$^+$, respectively. Si@N-graphene exhibits the charging and discharging capacities of 5517 and 2582 mAh/g, respectively, with a CE of 46.8 %. The far inferior CE of Si@N-graphene is ascribed to the residual functional groups decorating graphene edges, which may cause irreversible reactions in the first cycle. The capacity retentions measured at C/5 for both charge and discharge and corresponding CEs are presented in Figs. S6b & S6c, respectively. Si@N-graphene shows the highest capacities in the beginning of cycles, but suffers from rapid decay. After 50 cycles, Si@N-graphene shows 985.9 mAh/g with capacity retention of 61.9% from their initial values. When the C-rate sequentially increases from C/10 (=0.12 A/g) to 1C (=1.2 A/g) to 10C (= 12.1 A/g), Si@N-graphene exhibits inferior performance, as its capacity significantly decreases from 1882 mAh/g to 840 mAh/g to 311 mAh/g, respectively (see Fig S6e). In fact, this trend in the rate performance is opposite to the film conductivity in Fig. S2e. Despite the high electric transport via well-developed network of 2D graphene layers, less stable SEI layers caused by edge functional groups[6], as indicated by the lower CEs, hinders efficient Li ionic diffusion around the Si surfaces, limiting the overall rate performance. The lower CEs of graphene materials have been known to be associated with several features of graphene[7].[8] : 1) strong binding of Li ions with O- and H-containing functional groups and 2) large surface area. The results are in good agreement with previously reported graphene/Si composite anode materials.

In morphology, after 100 cycles, flexible N-graphene layers become significantly crumpled (arrow in Fig. S7c) and weakly bounded by pulverized Si particles after 100 cycles of Si@N-graphene, as shown in Figs. S7b & S7c. This signifies that repeated charge and discharge cycles significantly deteriorated the graphene-Si composite structure and leaded to the exposure of bare Si surface to the electrolyte. This subsequently lowers CEs compared to those of Si@N-CNT.

Experimental Section

Preparation of N-doped Graphene: Aqueous graphene oxide dispersion was prepared from commercially available graphite (Aldrich) by a modified Hummers method. After vacuum filtering with 10-fold-diluted hydrogen chloride (Sigma Aldrich, 37 %) several times, graphene oxide was vacuum dried at room temperature. The dried solid powder was redispersed in deionized water to remove residual ionic or acidic impurities by dialysis (Spectrum Laboratory, Inc., MWCO of membrane: 8000). The dialysis was performed for at least two weeks, occasionally changing the water in the glass bath. After dialysis, the resultant graphene oxide aqueous solution (3.0 mg/mL, 100 ml) was mixed with hydrazine monohydrate (Sigma Aldrich, N_2H_4 64~65%, reagent grade, 98 %) for N-doping. To increase doping amount, hydrazine pretreated samples were thermally reduced and N-doped with a H_2/NH_3 gas mixture at 750°C for 10 min.

Preparation of N-doped CNT: 500 mg of small diameter of CNT (Nanointegris, HiPco®, Pure grade) was sonicated in a 1:3 (32.5ml/97.5ml) mixture of HNO_3 (Junsei, extra pure) and H_2SO_4(Merck, 95~97%) for 10 h to generate oxygen functional groups; they were subsequently thermally treated at 400 °C for 40 min in air to remove any amorphous carbon species. For N-doping of CNTs, the oxygenated CNTs were thermally treated at 1100 °C for 4 h under a mixture gas flow of Ar (40 sccm) and NH_3 (60 sccm).

Graphitic Self-Encapsulation of Si : Prior to graphitic self-encapsulation, all graphitic carbons (undoped graphene, N-doped graphene, undoped CNT, and N-doped CNT) were dipped in deionized water (300mg/1L) for 1 h to enhance wettability. Graphitic self-encapsulation of Si was performed by mixing of black graphitic carbon dispersion (300 mg / 1 L solution of graphitic carbon in pH-controlled aqueous water) with an aqueous yellow brown Si

dispersion (2.7 g / 5 L solution of Si in pH-controlled aqueous water) under mild mechanical shaking at room temperature with a pH range of 1.5 to 9. The pH of the solution was controlled by addition of 1M HCl into the 28% ammonia solution. Under optimal assembly conditions, almost all graphitic carbon and Si participated in the form of graphitic self-encapsulated Si, leaving a transparent aqueous solvent. The resultant graphitic encapsulated Si was restored by vacuum-filtration, thoroughly rinsed with deionized water, and dehydrated 6 h at 80 °C in vacuum.

Characterization: The morphologies of Si, graphene, CNT, and graphitic encapsulated Si were characterized with field-emission scanning electron microscopy (FEI Magellan 400) and high resolution transmission electron micrsocopy (HR-TEM, FEI Titan G2 60~300 and Philips Tecnai F20). The EDS line scanning and spectra of the graphitic encapsulated Si were performed with corrected scanning TEM (JEOL JEM-ARM200F). A Zetasizer (Malvern, Zetasizer Nano ZSP) was used for the zeta potential measurements. TEM EDS and multipurpose XPS (Sigma Probe, Thermo VG Scientific) were used for the chemical analysis of graphitic encapsulated Si. The I-V curve of Si and graphitic encapsulated Si were measured by a four-wire sensing system (Keithley 2635 system). The surface area and porosity were measured with surface area analyzer (Micromeritics Tristar 2 3020) with the standard nitrogen system. The mass composition of Si and graphtic encapsulants was measured by Thermogravimetric analysis (TGA, Setaram) at N_2 atmosphere.

Electrochemical Characterization: The graphitic encapsulated Si was mixed with Super P and poly(acrylic acid) (PAA, Mw = 3,000,000, Aldrich) in the weight ratio of 70 (active) : 15 (binder) : 15 (Super P) and was then added into 1-Methyl-2-pyrrolidinone (NMP, Aldrich) to form a homogeneous slurry. The slurry was pasted onto the copper current collector (18 μm

thick Cu foil, Hohsen, Japan) using the doctor blade method. The pasted electrodes were dried in a vacuum oven at 70 °C for 9 h and punched into circular discs. All three kinds of samples in this work were prepared by the same conditions, and the active material loading density was ~0.8 mg/cm^2. CR2032 coin cells were assembled in an Ar-filled glove box. 1M LiPF$_6$ solution in a mixture of ethylene carbonate (EC) and diethyl carbonate (DEC) (1:1 = v/v, PANAX E-TEC, Korea) with fluoroethylene carbonate (FEC, 5 wt%, PANAX E-TEC, Korea) was used as the electrolyte. Celgard 2400 polypropylene films were used as separators. The galvanostatic charge and discharge method (same charge/discharge current) were applied in the voltage range of 0.005-1.2 V vs. Li$^+$/Li using a WBCS 3000 battery cycler (Wonatech, Korea).

Fig. S1
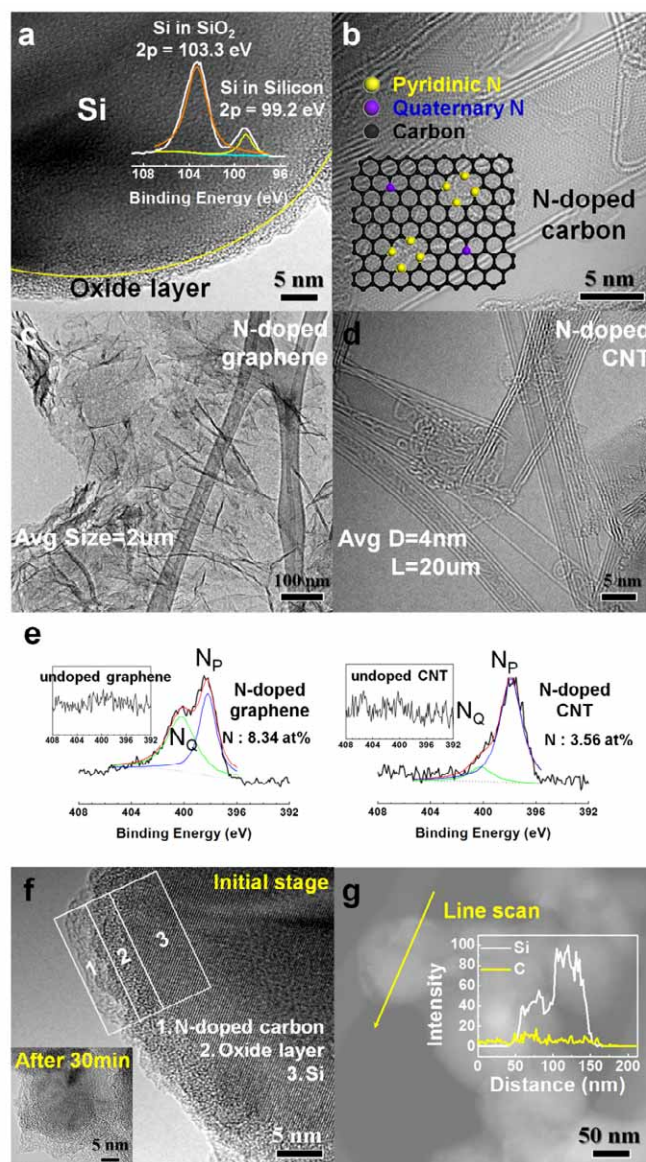
Fig. S1. (a) HR-TEM image and XPS spectra of Si particles. Boundary between Si and SiO$_2$ was indicated. (b) HR-TEM image of N-CNTs along with schematic illustration of N-doped sites. HR-TEM images of (c) N-graphene and (d) N-CNT. (e) N1s XPS spectra of N-doped carbon materials along with their undoped counterparts. (f) HR-TEM image of N-CNT encapsulated Si particles in the initial stage of mixing. (Inset) The same sample after mild stirring for 30 min. (g) EDS line scan over N-CNT encapsulated Si particle for elemental analysis profiles of Si and C.

Table S1

	undoped graphene	N-doped [1~2] graphene (8 at%)	undoped CNT	N-doped [3~5] CNT (4 at%)
R_S ($\Omega/\square$)	1,240	300	1,420	620
Φ (eV)	4.41	4.25	4.94	4.28
Water Contact Angle(°)	88	74	126.5	18

Table S1. Electrical and wetting properties of graphene and CNTs before and after N-doping.

Fig. S2
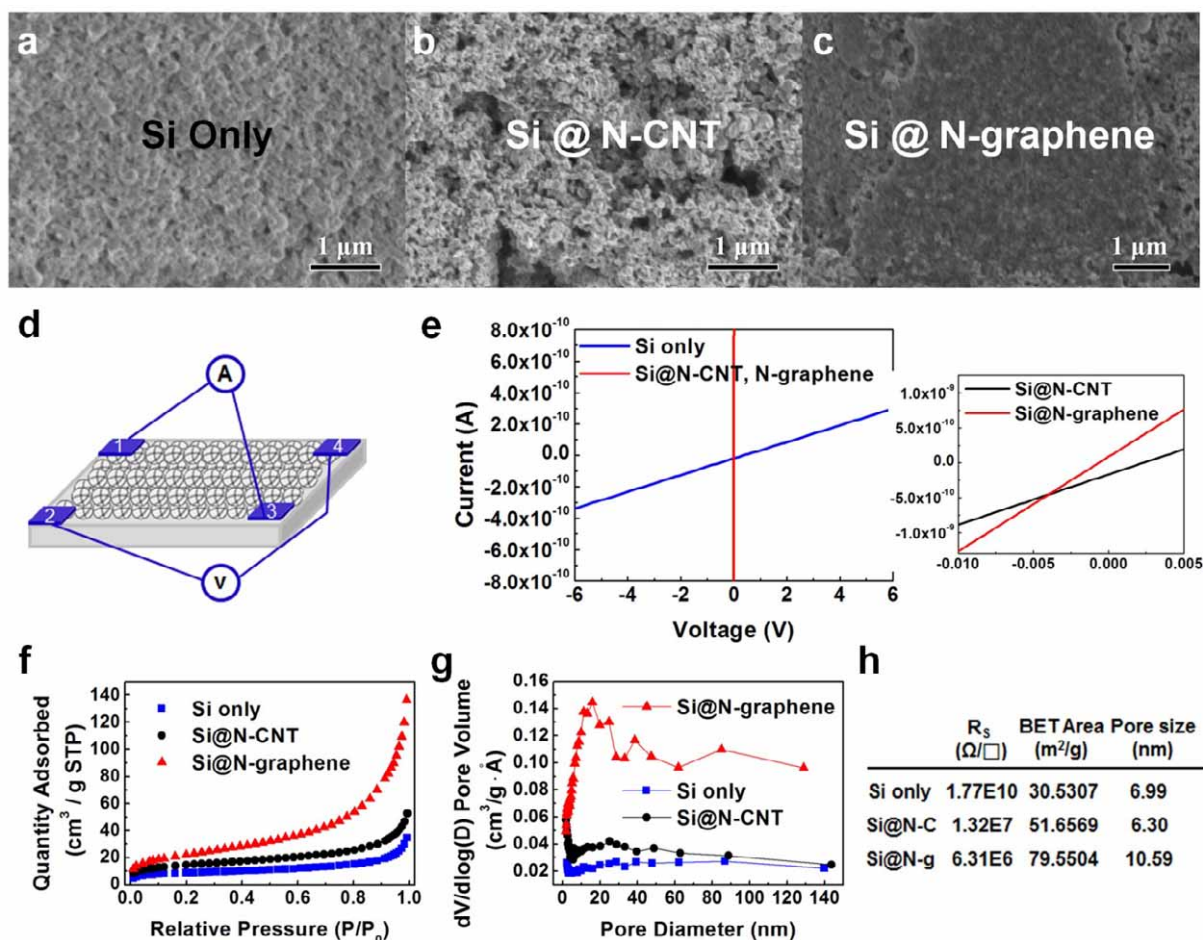
Fig. S2. Characterization of graphitic encapsulated Si in powder and film samples. SEM images of (a) pure Si, (b) Si@N-CNT, and (c) Si@N-graphene. (d) Schematic for four point probe method. (e) I-V curves of pure Si and Si@N-CNT. (f) N_2 adsorption-desorption isotherms and (g) BJH pore size distributions for pure Si, Si@N-CNT and Si@N-graphene. (h) Table summarizing the sheet resistances, surface areas, and average pore sizes of pure and encapsulated Si anodes.
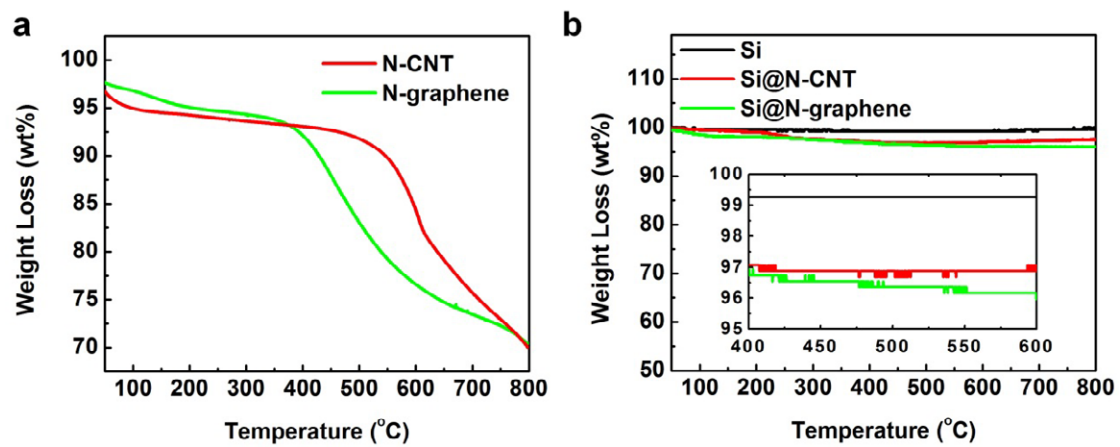
Fig. S3

Fig. S3. TGA weight loss curves for (a) N-CNT and N-graphene, (b) Si and graphitic carbon encapsulated Si.
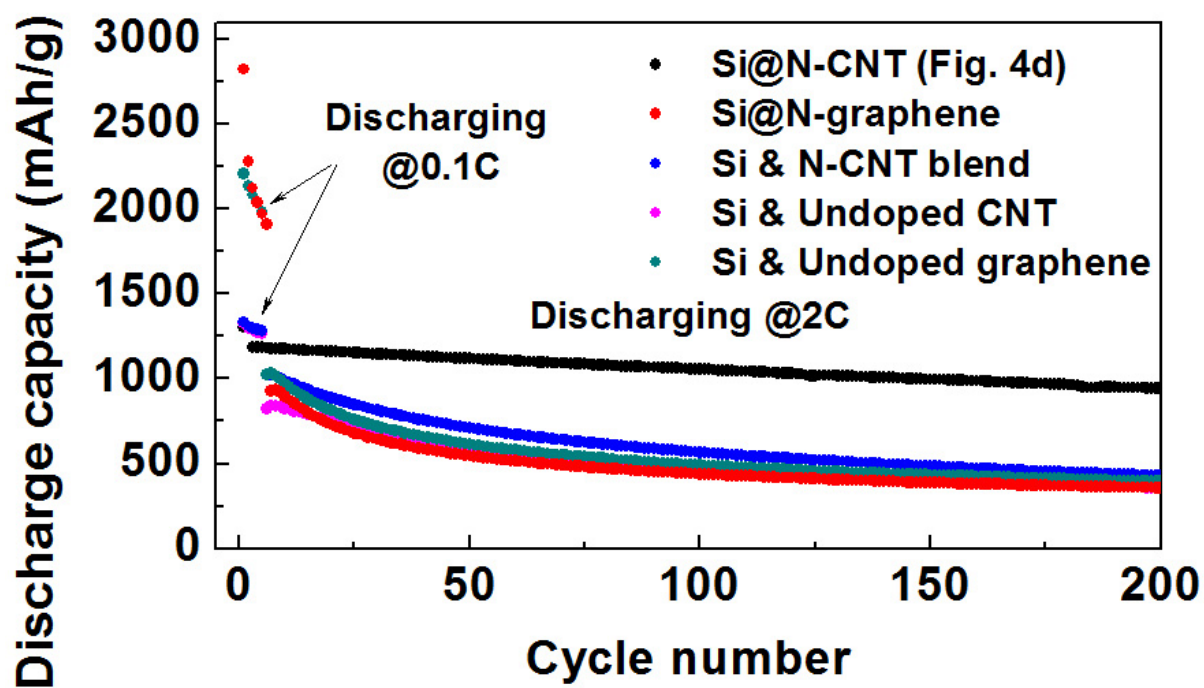
Fig. S4

Fig. S4. Reversible discharge capacities of various Si/graphitic carbon composites.
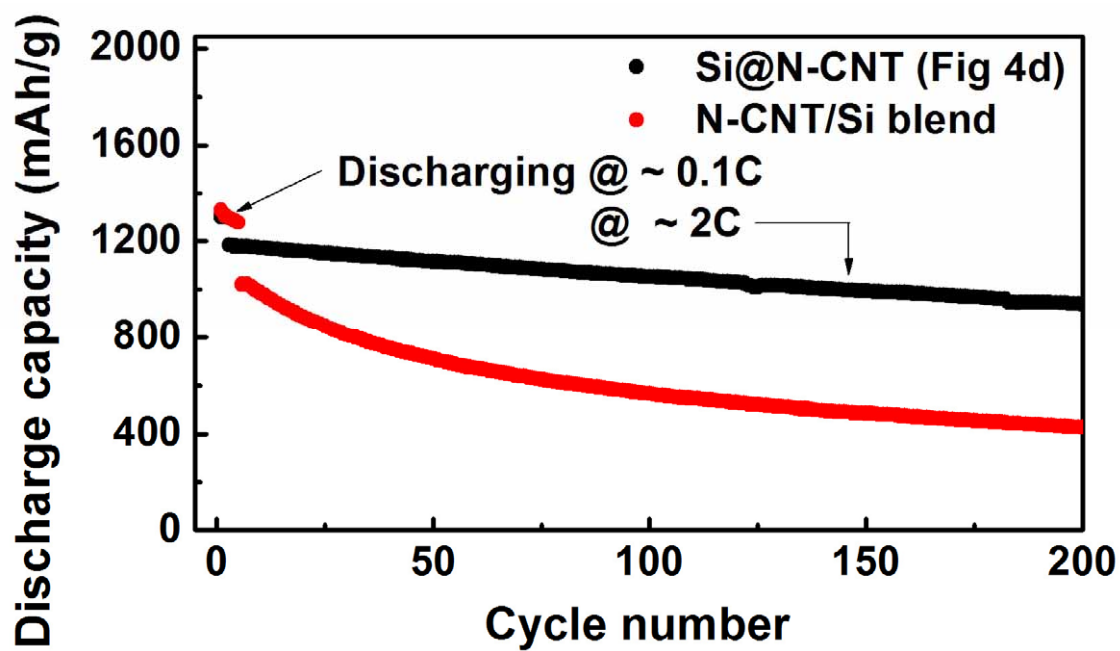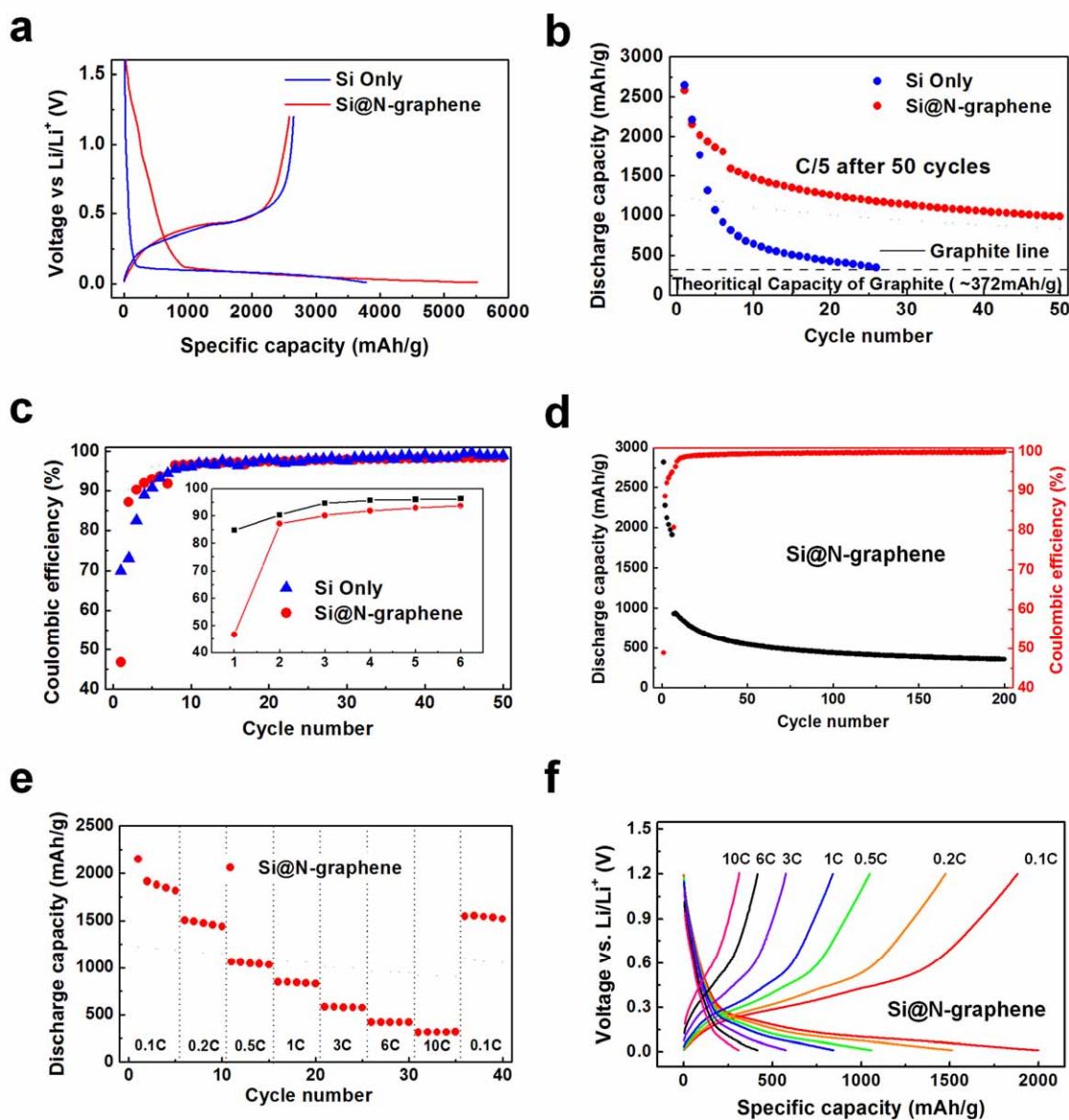
Fig. S5

Fig. S5. The cycling performance of Si@N-CNT and N-CNT/Si blend. Both were measured

at 0.1C (= 1300.8 mAh/g, 1306.8 mAh/g, respectively) for the first two cycles and then at 2C

(= 1180.1 mAh/g, 1022.7 mAh/g, respectively) for the subsequent cycles.

Fig. S6

Fig. S6. Electrochemical characterization of pure and graphene encapsulated Si anodes. (a) Potential profiles of pure Si, and Si@N-graphene during the first cycles at a C/10 rate. (b) Reversible discharge capacities and (c) Coulombic efficiencies during 50 cycles. (d) Cycling performance of Si@N-graphene measured at 2C. (e) Rate capability tests for Si@N-graphene at various C-rates. (f) Galvanostatic charge-discharge profiles of Si@graphene in the C-rate of C/10-10C. The gravimetric capacities are normalized with the total mass of Si and graphitic encapsulants.

Fig. S7
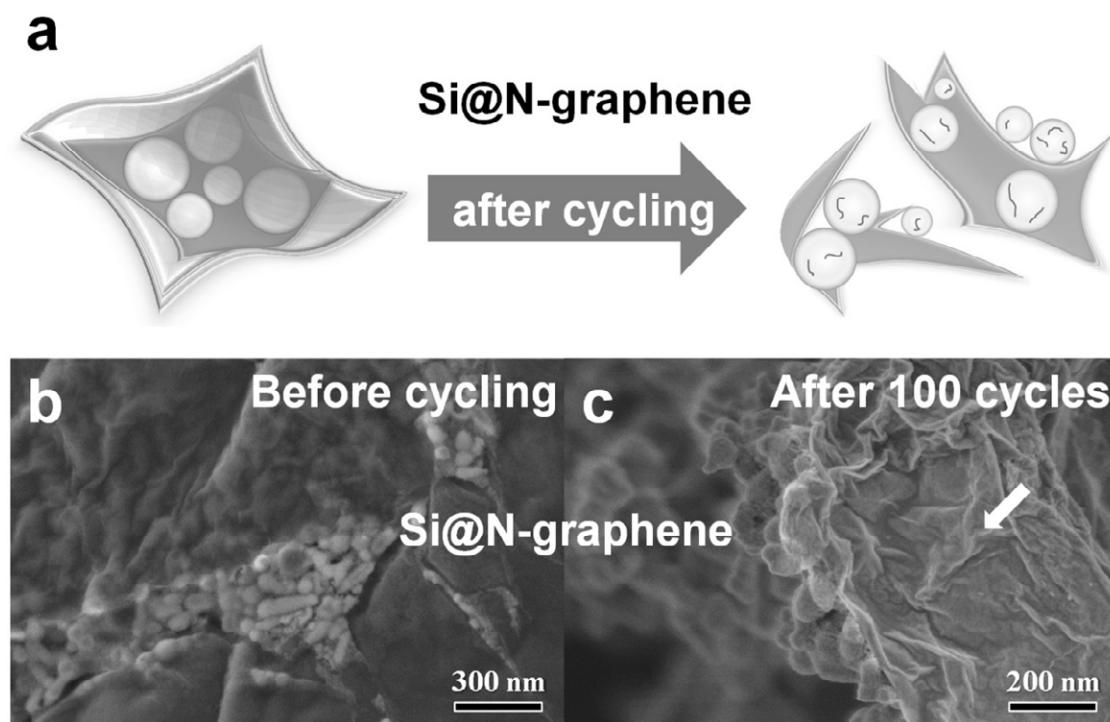
Fig. S7. Electrode morphology change before and after cycling. (a) Schematic illustration of electrode morphology change. HR-SEM images of Si@N-graphene (b) before and (c) after 100 cycles at 1C.

REFERENCES

[1] D. H. Lee, W. J. Lee and S. O. Kim, *Nano Lett.* 2009, **9,** 1427-1432.

[2] J. O. Hwang, J. S. Park, D. S. Choi, J. Y. Kim, S. H. Lee, K. E. Lee, Y. –H. Kim, M. H. Song, S. H. Yoo and S. O Kim, *ACS Nano* 2012, **6**, 159-167.

[3] D. H. Lee, W. J. Lee, W. J. Lee, S. O. Kim and Y. -H. Kim, *Phys. Rev. Lett.* 2011, **106**, 175502.

[4] S. H. Lee, H. W. Kim, J. O. Hwang, W. J. Lee, J. Kwon, C. W. Bielawski, R. S. Ruoff, and S. O. Kim, *Angew. Chem. Int. Ed.* 2010, **49**, 10084-10088.

[5] W. J. Lee, J. M. Lee, S. T. Kochuveedu, T. H. Han, H. Y. Jeong, M. Park, J. M. Yun, J. Kwon, K. No, D. H. Kim and S. O. Kim, *ACS Nano* 2012, **6**, 935-943.

[6] M. E. Spahr, H. Wilhelm, T. Palladino, N. Dupont-Pavlovsky, D. Goers, F. Joho and P. Novák, *J. Power Sources* 2003, **119-121**, 543-549.

[7] F. Sun, K. Huang, X. Qi, T. Gao, Y. Liu, X. Zou, X. Wei and J. Zhong, *Nanoscale* 2013, **5**, 8586-8592.

[8] K. Evanoff, A. Magasinski, J. Yang and G. Yushin, *Adv. Mater.* 2011, **1**, 495-498.